THE JOURNAL OF PHYSICAL CHEMISTRY C

Article

pubs.acs.org/JPCC

Structure and Phase Behavior of a Discotic Columnar Liquid Crystal Confined in Nanochannels

Carole V. Cerclier,[†] Makha Ndao,[†] Rémi Busselez,[†] Ronan Lefort,[†] Eric Grelet,[‡] Patrick Huber,[§,∥] Andriy V. Kityk,[⊥] Laurence Noirez,[#] Andreas Schönhals,[∇] and Denis Morineau[*,†]

[†]Institut de Physique de Rennes, CNRS UMR 6251, Université de Rennes 1, 35042 Rennes, France

[‡]Centre de Recherche Paul-Pascal, CNRS UPR 8641, Université de Bordeaux 1, 33600 Pessac, France

[§]Experimental Physics, Saarland University, 66041 Saarbrücken, Germany

[∥]Materials Physics and Technology, Hamburg University of Technology, 21073 Hamburg, Germany

[⊥]Faculty of Electrical Engineering, Czestochowa University of Technology, 42-200 Czestochowa, Poland

[#]Laboratoire Léon Brillouin (CEA-CNRS), CEA Saclay, 91191 Gif sur Yvette, France

[∇]BAM Bundesanstalt für Materialforschung und −prüfung, 12205 Berlin, Germany

ABSTRACT: The confinement of discotic columnar liquid crystal in nanoporous templates is a promising strategy to design nanofibers with potential applications in organic electronics. However, for many materials, geometric nanoconfinement has been shown to induce significant modifications of the physical properties, such as structure or phase behavior. We address the case of a discotic columnar liquid crystal confined in various templates. The influence of the size, the roughness, and the chemical nature of pores was investigated for a pyrene derivative by small-angle neutron scattering, X-ray diffraction, and calorimetry on a wide range of temperatures. A homeotropic anchoring (face-on orientation of the disk-shape molecules at the interface) is favored in all smooth cylindrical nanochannels of porous alumina while surface roughness of porous silicon promotes more disordered structures. The hexagonal columnar−isotropic phase transition is modified as a result of geometrical constraints and interfacial interactions.

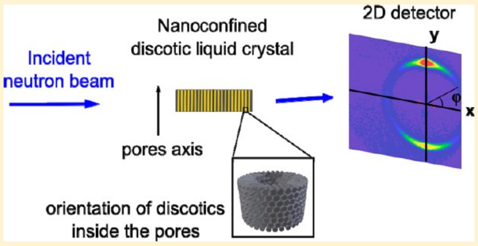

■ INTRODUCTION

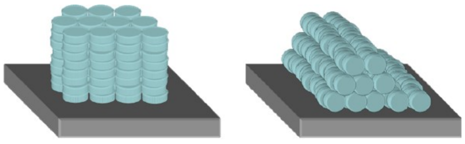

Figure 1. Schematic representation of the different orientations of a discotic columnar liquid crystal with regard to a surface.

Organic electronics is a field of intense scientific activity because of promising applications toward the fabrication of effective low-cost, portable and disposable devices such as organic light emitting diodes, photovoltaic devices, field effect transistors, memory elements or sensors.[1] Among organic semiconductors, discotic columnar liquid crystals (DCLC) are a promising class of materials,[2,3] which consist of disklike molecules composed of a rigid aromatic core surrounded by flexible aliphatic chains. These molecules self-assemble by stacking on top of one another and form columns, which arrange in a regular 2D lattice.[4] DCLC combine unique material properties, such as fluidity and the self-healing of structural defects with anisotropic mechanical and optical properties. Thanks to their self-organization, a strong orbital overlap occurs in one dimension and allows charge carriers to move easily along the columns. Thus, depending on potential applications, a large effort is required to control the parameters that influence the alignment mechanism in the suitable geometry for devices. Two different possible organizations of columns at the solid surface are illustrated in Figure 1 and correspond respectively to the homeotropic (face-on orientation of the molecules) and the planar (edge-on orientation of the molecules) anchoring conditions. To obtain efficient photovoltaic cells, columns must form a homeotropically (face-on) aligned open film on the surface of one electrode prior to deposit the second electrode.[5]

Usually, columns exhibit planar (edge-on) alignment in open thin films,[6,7] while they align homeotropically when sandwiched between two solid substrates.[7] The organization results from the competition between homeotropic and planar alignment due to the difference in interfacial tensions between air/liquid crystal and liquid crystal/substrate.[8] Several works have reported on homeotropic alignment of hexagonal DCLC in thin films[9−13] and the strategies for homeotropic alignment were the controlled thermal annealing of DCLC in open film or in confined geometry between two interfaces,[8,11,12,14,15] or the

Received: April 17, 2012
Revised: August 21, 2012
Published: August 22, 2012

combination of two miscible mesogens exhibiting different columnar mesophases.[13] One possible breakthrough in the field of molecular electronics could emerge from the manufacturing of ordered DCLC nanowires. The possible formation of DCLC nanowires has already been reported by Steinhart and co-workers.[16] Nanowires are produced by impregnation of molecular materials in anodic alumina oxide (AAO), which is a prototypical nanoporous template with cylindrical aligned nanochannels.

While obtaining self-assembled semiconducting organic nanowires is appealing from a technical point of view, it is noteworthy that the introduction of geometrical nanoconfinement raises many questions of fundamental interest. Nanoscale confinement induces significant changes in the physical properties of simple molecules[17,18] due to the chemical and physical properties of the interface and the size and the dimensionality of the confining topology. In the case of liquid crystals, previous studies on calamitic rodlike mesogens in nanopores[19−23] have shown that most of the fundamental properties of the confined phases are deeply affected by confinement. Moreover, new features, which are qualitatively different from the bulk case, are observed: the bulk phase transitions are suppressed, and new paranematic, short-range ordered smectic, or low-temperature layered structures are observed.

As a consequence, one expects that nanoconfined DCLC properties may radically depart from their bulk counterparts. Up to now, only few studies have investigated the effects of confinement on the morphology and/or the thermodynamics of DCLC.[16,24−26]

The objective of this work was to identify how confinement affects both structure and the phase diagram of a DCLC. The effects of confinement were probed by small-angle neutron scattering and X-ray diffraction using a pyrene derivative as model DCLC system. The influence of several parameters such as the size of channels, the chemical nature of nanoporous membranes and the roughness of the interface was investigated. Results of this study may bring a new insight on the nanoconfinement of discotic columnar liquid crystals and may help to design DCLC/template systems to fabricate adequately aligned DCLC nanowires.

■ EXPERIMENTAL PART

Liquid Crystal. The discotic molecule used to investigate the behavior of columnar liquid crystal in confinement was the pyrene 1,3,6,8-tetracarboxylic *rac*-2-ethylhexyl ester (Py4CEH). It consists of a polyaromatic core surrounded by flexible aliphatic chains. Synthesis details of this molecule are described elsewhere.[27]

Anodized Aluminum Oxide (AAO) Nanoporous Membranes. Anopore membranes with pores of 200 nm in diameter were provided by Whatman. The other membranes were synthesized from annealed aluminum foils (purity: 99.99%) provided by Alfa Aesar. Samples were first cleaned with acetone and then electropolished in a solution of ethanol and perchloric acid (60%) (75:25). Afterward, a double anodization was performed in a thermally isolated electrochemical cell under constant voltage. The main parameters involved in anodization are the output voltage, the electrolyte, and the temperature.[28−31] Two different procedures were chosen depending on the expected diameter of pores. Parameters used to obtain pores of either 25 or 50 nm in diameter (standard deviation: 5 nm) are listed in Table 1. Characterization of samples was made by scanning electron microscope (JEOL JSM 6301F) and transmission electron microscope.

Table 1. Anodization Parameters Used to Produce AAO Membranes

expected diameter (nm)	output voltage (V)	electrolyte	temperature (°C)
25	40	0.3 M oxalic acid	5
50	20	10%w sulfuric acid	−5

Grafting of Membranes. Membranes were first cleaned and dried at 403 K under vacuum for 5 h. Then they were plunged into hexamethyldisilazane (Fluka, Analytical) and placed in a reflux setup at 323 K for 21 h. Samples were sonicated during 2 min in acetone, rinsed and dried at 323 K until use.

Etching of Silicon. Porous silicon layers were produced from polished p^+-type (100) oriented silicon substrates (300 μm thick, 3 in. in diameter, 0.003−0.007 Ω). Silicon wafers were electrochemically etched in a solution of ethanol mixed with hydrofluoric acid (20%) (60:40), using a platinum working electrode and an electrochemical cell under constant current of 240 mA. Etching was achieved for two hours to obtain 100 μm thick porous layers.

Confinement. Py4CEH was confined into nanoporous samples by spontaneous imbibition in the liquid phase. Membranes were dried at 403 K under vacuum for several hours prior to use. Then, filling was achieved under Py4CEH vapor pressure in a vacuum chamber at a temperature of 403 K, above the $\mathrm{Col_h}$-Iso transition, in order to accelerate the filling of the pores by capillary action. The excess of liquid crystal was removed by squeezing the samples between Whatman filtration papers.

Small-Angle Neutron Scattering (SANS). Measurements were performed at the Laboratoire Léon Brillouin (Saclay, France) on the SANS spectrometer PAXY. The surface of the membranes was oriented parallel to the incident beam with axis of the pores perpendicular to the beam and aligned vertically. Spectrometer was configured with a wavelength of 3.5 Å and a sample-to-detector distance of 1.1 m which corresponds to a total q-range from 0.1 to 0.7 $\mathrm{Å}^{-1}$. Data processing was performed with the program PAsiNET developed by the Laboratoire Léon Brillouin. Neutron scattering patterns were scanned from 330 to 370 K during both heating and cooling stages. Temperature was controlled with a homemade oven and heating/cooling rates were less than 0.1 $\mathrm{K{\cdot}min^{-1}}$.

X-ray Scattering Setup. Experiments were performed at ambient temperature using a Rigaku rotating anode generator at a wavelength of 1.54 Å (Cu K-alpha emission). Diffraction patterns were recorded in transmission, with a 2-dimensional detector located at 133 mm from the sample. Samples were oriented so that the incident X-ray beam was parallel to the membrane pores, i.e., along the lowest dimension of the membrane to maximize the transmittance. In this configuration, the range of scattering wave vector is from 0.17 to 2.0 $\mathrm{Å}^{-1}$. Temperature was controlled with an in-house made heating stage having an accuracy of 0.01 K, and the average applied heating/cooling rates were 0.01 $\mathrm{K{\cdot}min^{-1}}$ (including exposure time at each temperature).

Differential Scanning Calorimetry (DSC). The calorimetric scans were performed from a differential scanning calorimeter (DSC Q100, TA Instruments) for three different rates (5, 10 and 20 K·min^{-1}). To quantify ramp rate effects and disentangle kinetic effects from genuine supercooling, the columnar−isotropic transition temperatures were determined by extrapolation to zero ramp rate. Therefore, they could be compared with the transition temperatures observed in neutron and X-ray scatterings performed at very small rate (quasistatic equilibrium).

■ RESULTS AND DISCUSSION

Texture of Bulk Py4CEH. The pyrene derivative exhibits a hexagonal columnar mesophase (Col$_h$) at ambient temperature. This columnar phase transforms to the isotropic liquid phase (Iso) at $T_{\mathrm{Col_h-Iso}}$ = 365 K, which allows thermal processing and technological applications in a convenient range of temperatures.[32] Prior to confinement studies, the liquid crystal was characterized in the bulk state by SAN and X-ray scatterings.

Figure 2 displays two-dimensional spectra of neutron scattering obtained for Py4CEH either in the isotropic phase (365 K) or in the columnar phase (330 K). At 365 K, the pattern exhibited a broad ring of low intensity, which is characteristic of the diffuse scattering from the low range intermolecular interactions in the isotropic liquid phase. This ring becomes thinner and much more intense in the hexagonal columnar mesophase than in the isotropic phase. This two-dimensional circular pattern corresponds to a spherical symmetry, which is the signature of numerous columnar domains without preferential orientation. Moreover, the ring is located at an angle of diffraction corresponding to a momentum transfer $q_{100} \approx 0.35$ Å^{-1}. This value is coherent with X-ray diffraction experiments (Figure 3a) and previous reported results[11,12] and is assigned to the (100) Bragg reflection peak of the hexagonal array of columns.[12,32] X-ray scattering spectra of bulk Py4CEH in columnar phase (Figure 3a) allows observing high-order reflections, such as (110) and (210), the liquidlike order of the aliphatic chains (1.4 Å^{-1}) but also the interdisk reflection (001) or π-stacking at about 1.8 Å^{-1}.

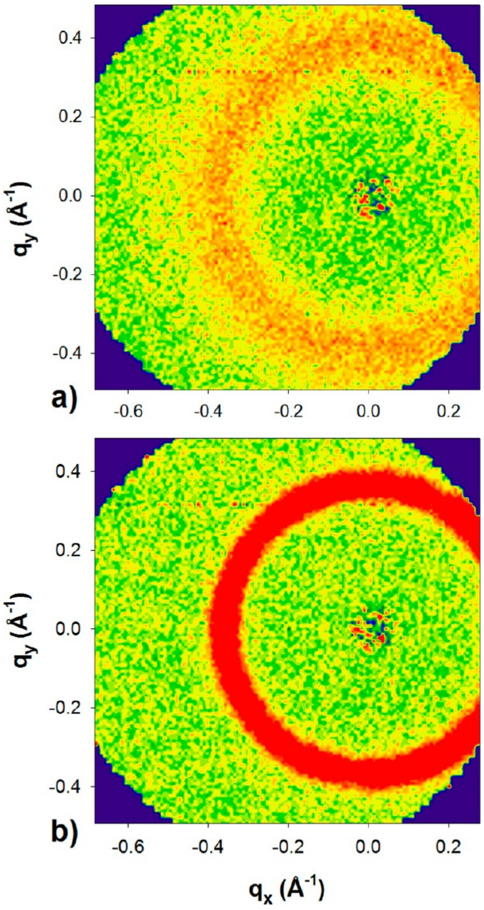

Figure 2. Two-dimensional neutron scattering patterns displayed by bulk pyrene derivative at (a) 365 K in the isotropic phase and at (b) 330 K in the columnar phase. The circle in the middle of the ring is the mark of the beam trap.

Effect of the Nature of Confining Materials on the Py4CEH Texture. To explore how confinement influences the self-organization of columnar liquid crystals, Py4CEH was embedded into cylindrical nanopores of AAO or porous silicon (pSi) characterizing by different pore diameters. AAO membranes are composed of parallel cylindrical channels obtained by electrochemical etching.[33] Depending on etching conditions, the pore diameter varies from 20 to hundreds of nm. A typical micrograph of AAO is shown in Figure 4. Membranes with three different pore sizes (200, 50, and 25 nm) were selected for our investigations and were referred hereafter as AAO200, AAO50, and AAO25, respectively. We emphasize here that hydroxyl moieties present on the alumina surface make AAO membranes hydrophilic. This surface interaction was also tuned by chemical grafting of the pores with trimethylsilyl groups, resulting in a more hydrophobic surface than native alumina. In comparison to AAO, pSi corresponds to the case of highly rough[34] and hydrophobic channels combined with a smaller pore size (8 nm) than those of AAO.

Figure 3b presents the integrated X-ray spectrum of Py4CEH confined in AAO50. High-order reflections are no longer visible except the (200) peak which can be detected. On the contrary, the first-order Bragg peak (100) and the π-stacking reflection remain intense without significant shift. It is however broader in AAO50 (fwhm = 0.025 Å^{-1}) than in the bulk (fwhm = 0.012 Å^{-1}), which illustrates the reduction of the correlation length induced by confinement. The presence of the π-stacking signal in normal incidence diffraction geometry suggests that columns are aligned perpendicularly to the incident X-ray beam and so to the cylindrical pores. This homeotropic anchoring (face-on) is further confirmed by the two-dimensional spectra obtained by neutron scattering for confined Py4CEH at 300 K (cf. Figure 5). The texture corresponding to the observed X-ray and neutron diffraction patterns can be expressed as a radial distribution of the column axes perpendicular to the pore axis with a face-on (homeotropic) surface anchoring condition. Indeed, all spectra of liquid crystal confined in AAO were composed of a weak isotropic ring at q_{100} superimposed by two intense spots sitting in the vertical axis, i.e., in the direction parallel to the pore axis. Accordingly, this diffraction pattern is consistent with a radial organization of the confined columnar phase associated to a homeotropic anchoring. This possible organization is sketched in Figure 5f. It assumes that the axis of columns is perpendicular to the surface of pores and displays an azimuthal degeneracy of the hexagonal symmetry with respect to the normal surface (x-axis in Figure 5f). In this picture, one has to consider an additional cylindrical powder average with respect to the pore axis (y-axis in Figure 5f). The diffraction

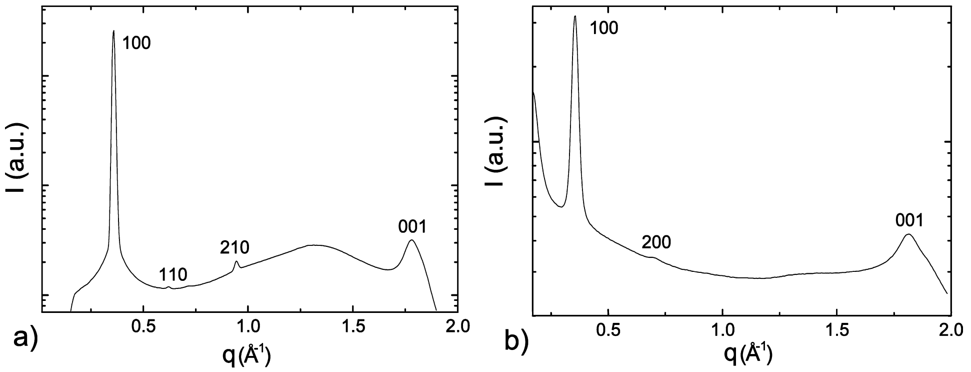

Figure 3. X-ray diffractograms of the pyrene derivative probed (a) in bulk at 355 K and (b) confined in AAO50 at 298 K.

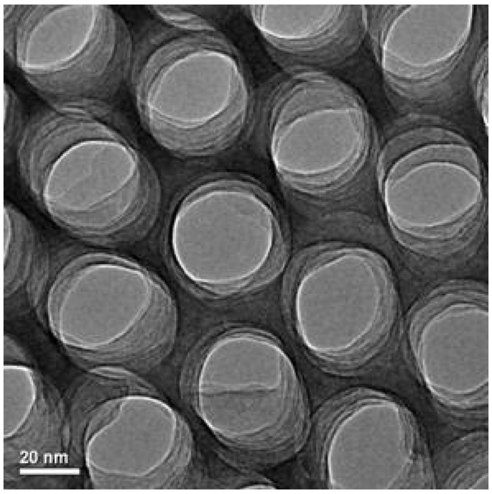

Figure 4. TEM micrograph of AAO with pores 25 nm in diameter.

pattern of each homeotropically anchored domain consists of two vertical Bragg spots, except for the fraction of columns that are parallel to the incident beam. In this case, they are associated to the isotropic ring due to the azimuthal degeneracy. It cannot be excluded that isotropic diffraction or diffuse scattering from randomly aligned or defective columnar domains could additionally contribute to this weak isotropic diffraction ring. Indeed, the homeotropic anchoring in cylindrical confinement is not compatible with a defect free structure and disorder is expected in the pore center. The analysis of the width of the diffraction peak provides a better insight into the nature of the column ordering as discussed later. Considering now the conditions of confinement, it appears that the nanometric size of channels or the presence of a hydrophobic interface does not affect the homeotropic anchoring of the liquid crystal. It is consistent with previous studies[2,7,10,15] which report on the homeotropic alignment of DCLC in hexagonal columnar mesophase when they are sandwiched between two solid substrates.

Interestingly, a quite different situation is encountered in the case of porous silicon (diameter of 8 nm). The neutron spectrum presents an isotropic ring instead of vertically aligned Bragg spots (Figure 5e). This pattern is typical of a powder diagram, which suggests that the preferential homeotropic anchoring observed for AAO is not present anymore in the case of porous silicon. This diffraction ring could also originate from the formation of more disordered domains, with a structure exhibiting only short-range positional order. Both contributions are expected to be favored by the strong surface roughness of silicon channels[34] that induces a large amount of quenched disorder.[19,20,35,36]

The intensity was then integrated radially as a function of the azimuthal angle φ (Figure 6) for Py4CEH confined either in nongrafted AAO or in porous silicon. As it was already observed in 2D spectra, two symmetric structural peaks stand at 90° or −90°, which correspond to the long axis of the channels. We can also observe a dip around 0°, which results from the large absorption of the neutron beam in the horizontal plane of the membranes. The two symmetric vertical peaks are observed only for Py4CEH confined in the AAO matrices, and their intensity decreases with the pore size. We have checked that this decrease is not attributed to a difference in amount of confined material for each sample. Indeed the porous volume was estimated from the analysis of scanning electron micrographs and found to be comparable for all the AAO (Table 2) and could not account for the observed variation in diffracted intensity. The variation of the integrated Bragg intensity with the pore size is shown in the inset of Figure 6 and exhibits a systematic decrease with the pore diameter. A linear extrapolation of this decrease predicts a vanishing intensity of the diffraction peak for a pore size smaller than 10 nm. This result is consistent with the diffraction pattern observed for porous silicon, with a pore diameter of 8 nm. In the largest pores, the hexagonal arrangement of the columns induced by a homeotropic anchoring can obviously develop from the surface. Nevertheless, the formation of a fully ordered domain could not occur inside the entire volume of pores. This phenomenon induces a topological frustration arising from the incompatibility between the surface homeotropic anchoring condition and the cylindrical pore symmetry, which was also discussed for calamitic LC confined in pores of different symmetry.[37] In the smallest pores, the increasing surface curvature gradually restricts the volume of homeotropically aligned domains, which are submitted to ever-increasing elastic distortions. These findings were also evidenced by Steinhart and coworkers[16] in the case of a triphenylene derivative confined in an alumina template.

We focus now on the AAO50 sample with two different surface properties (i.e., native and grafted AAO). The objective is to better understand how the nature of the surface interaction could influence the organization of confined Py4CEH. The structural peak is around twice as intense for the grafted Py4CEH-AAO50-CH3 sample as those of the native Py4CEH-AAO50 sample. Moreover, we can observe on the grafted sample a doublet of shoulders located on both sides of the main structural peak at ±60° and ±120° (Figure 7). The same

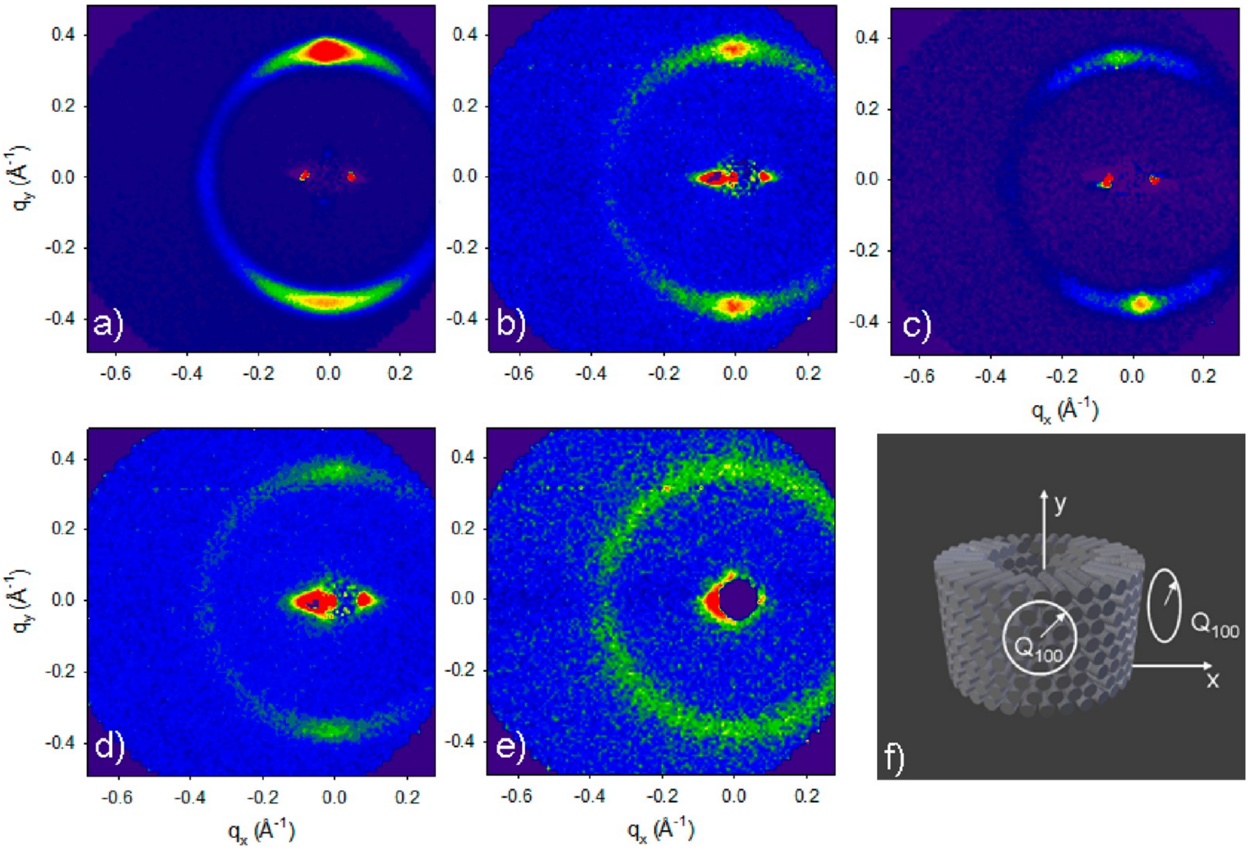

Figure 5. Two-dimensional neutron scattering patterns of Py4CEH confined in (a) AAO200; (b) AAO50; (c) grafted AAO50; (d) AAO25; and (e) porous silicon (8 nm). (f) Schematic representation of the organization of DCLC in pores. *y* and *x* axes correspond, respectively, to the direction along nanopores and to the plane of membranes. The anisotropic central scattering observed close to the beam trap is due to the scattering of nanoporous membranes.

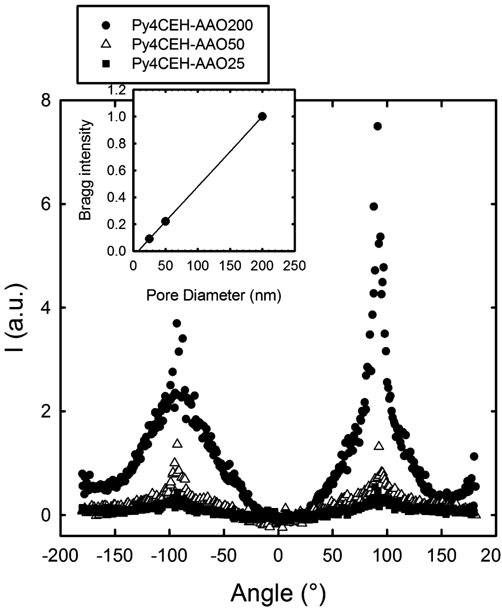

Figure 6. Azimuthal representation of the distribution of the neutron scattering intensity for pyrene derivative confined in AAO200, AAO50, and AAO25 membranes. Inset: the normalized integrated intensity of Bragg peak is represented as a function of pore diameter.

feature has also been observed for the grafted AAO200 (results not shown). The position of these additional peaks corresponds to a 6-fold symmetry. These peaks could indicate that the hexagonal symmetry of the column axis laying perpendicular to the pore surface is not completely averaged with respect to the normal vector to the surface. The (100) crystalline direction of the DCLC would be preferentially aligned along the pore axis. A preferred orientation of a crystalline direction along the nanochannel axis has been observed for *n*-hexane,[38] other medium-length *n*-alkanes,[39] and *n*-alcohols.[40] According to these studies, a preferred orientation of the pore crystals could be related to a nanoscale analogous of the Bridgman-type process, where the crystal axis corresponding to the direction of fastest crystal growth aligns along the axis of channels. A comparable mechanism has been invoked to interpret the thermal switching of molecular alignment in the smectic phase of a rodlike nematogen confined in AAO.[20] Note that in all cases, the thermal history of the sample can strongly influence the domain orientation and size, especially the cooling rate used to grow the liquid crystal from the isotropic liquid phase.

Phase Transition under Confinement. The neutron diffraction patterns of bulk pyrene derivatives were studied during heating and cooling in a temperature range from 370 to 330 K. After radial integration of the 2D spectra, the structural peak was fitted with a Gaussian function. The normalized intensity, peak position and width of the peak are presented as a function of temperature in Figure 8. A sudden change of these characteristic quantities is observed at 364 K. On cooling, the columnar−isotropic transition is characterized by an abrupt increase of the normalized diffraction peak intensity from 0.2 to 1. Meanwhile, the peak position shifts slightly to lower q values from 0.38 to 0.35 Å^{-1} and its full width at half-maximum

Table 2. Characteristics of AAO Membranes

	porosity (%)	pore density (μm^{-2})	porous volume (mm^3)	surface of channels (mm^2)	S/V (m^{-1})	I_{peak} (au.) (see Figure 6)
AAO200	40[a]	12.3[a]	2.4	4.64×10^4	1.93×10^4	1
AAO50	24	105	3.3	2.79×10^5	8.45×10^4	0.22
AAO25	20	354	3.8	6.41×10^5	1.69×10^5	0.09

[a] Values from ref 51.

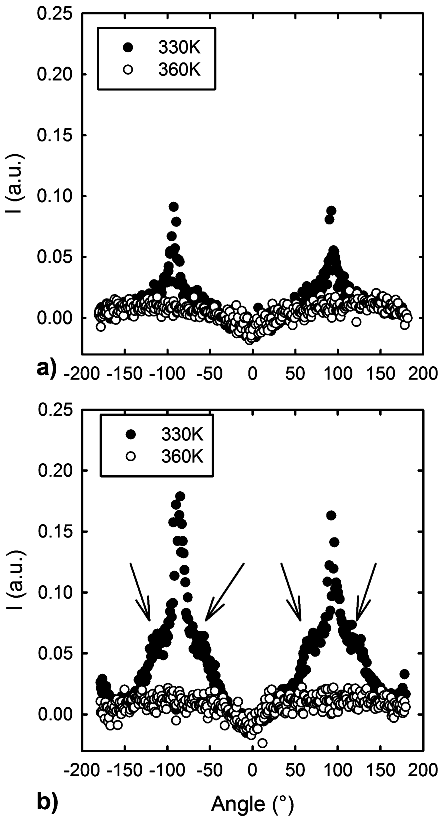

Figure 7. Azimuthal representation of the distribution of the neutron scattering intensity for pyrene derivative confined in (a) native AAO50 and (b) grafted AAO50.

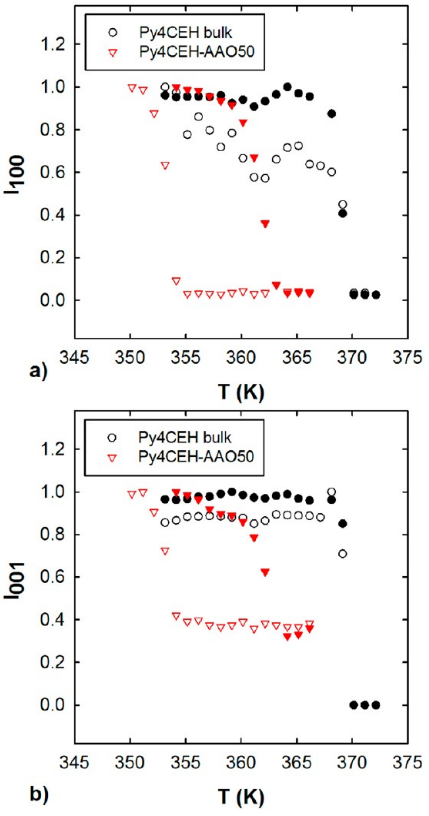

Figure 9. Intensity of 100 intercolumnar (a) and 001 interdisc (b) peaks observed by X-ray scattering as a function of temperature. The intensity is normalized to the maximum intensity of the respective reflections. Empty (full) symbols correspond to measurements performed during cooling (heating).

(fwhm) sharpens from 0.065 to 0.02 Å^{-1}. The analysis of X-ray diffraction pattern allowed us to probe the intensity of both intercolumnar (100) and interdisc (001) peaks as a function of temperature (Figure 9) because of the wider range of q available with our X-ray diffraction setup compared to the SANS one. The intensity of both peaks follows the same behavior with an abrupt increase when the columnar phase is

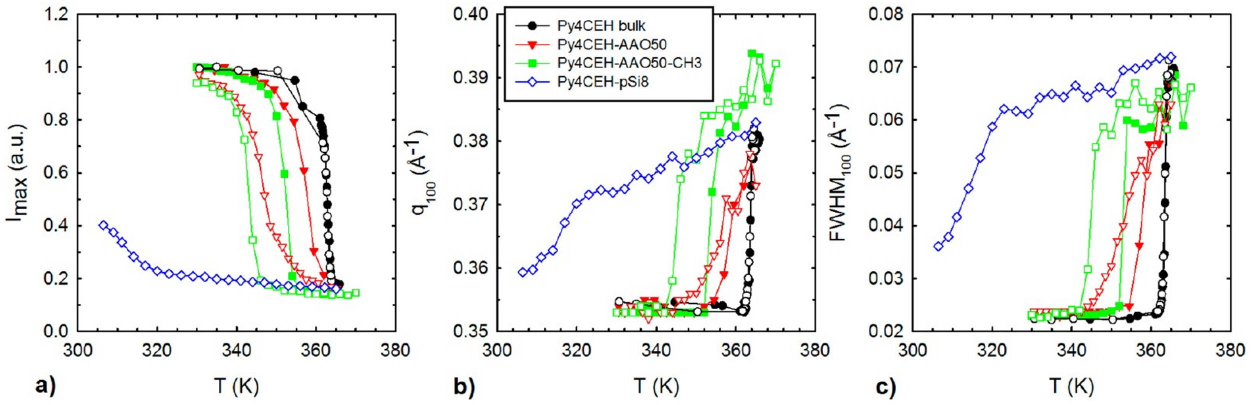

Figure 8. Comparison of Col$_h$−Iso transition of confined and bulk liquid crystal (a) normalized I_{max}; (b) position of peak (q_{100}); (c) fwhm of peak. Empty (full) symbols correspond to measurements performed during cooling (heating).

reached, associated to a concomitant formation of columns and intercolumnar order. These discontinuous changes together with the small hysteresis observed by DSC (about 0.5 K, see Table 3) are consistent with a first-order character of the Col$_h$−Iso transition of Py4CEH..

Table 3. Temperatures of Columnar−Isotropic Transition for Bulk and Confined Py4CEH Determined from Neutron and X-ray Scatterings and DSC Experiments (Extrapolated to a Zero Ramp Rate)[a]

		bulk	AAO50	Grafted AAO50
heating (ΔT_m)	SANS	364	359 (−5)	354 (−10)
	X-ray	369	362 (−7)	
	DSC	364.5	357 (−7.5)	354 (−10)
cooling (ΔT_f)	SANS	364	345 (−19)	342 (−22)
	X-ray	369	353 (−16)	
	DSC	364	350 (−14)	348 (−16)
$\Delta T_m/\Delta T_f$	SANS		0.26	0.46
	X-ray		0.44	
	DSC		0.50	0.62

[a] All temperature values are expressed in Kelvin. Values in brackets correspond to the difference of transition temperature between bulk and confined samples.

Similar to bulk Py4CEH, the Col$_h$−Iso transition of confined DCLC is accompanied by an increase in intensity and a sharpening of the columnar peak on cooling both in neutron (parts a and c of Figure 8) and X-ray scattering (Figure 9). In addition, the transition is shifted toward lower temperatures with regard to the bulk sample (Table 3). This negative shift increases with the decrease of pores size and eventually reaches about 50 K in the case of porous silicon. Moreover for the AAO membranes, a temperature hysteresis loop is observed, which was not observed for the bulk system with scattering methods. Note that for the pyrene derivative confined in pSi, the intensity was recorded only on cooling.

Modifications of the phase behavior have already been observed for a variety of molecular systems, comprising both low-molecular weight glass-forming liquids[41,42] and calamitic liquid crystals.[43,44] They can be considered as salient effects of mesoporous confinement for systems with varying molecular complexity.

A point of interest is the depression of the transition temperature of the confined materials. The downward shift of the Col$_h$−Iso transition temperature measured by SANS is $\Delta T = -5$ K for the AAO50. The value can be compared with the case of calamitic liquid crystals: about −2 K for the nematic-to-isotropic transition for 5CB in a AAO porous membrane with the same pore size.[45] A probable origin of this observation is related to the dominance of interfacial energy with decreasing the pore size. This feature has been usually expressed by the Gibbs−Thomson equation for the variation of the melting temperature with the pore size.[46] In the case of liquid crystals, one might also invoke the concomitant effect of the elastic energy and/or the formation of topological defects. The existence of columnar order in the channels with a homeotropic anchoring requires elastic distortion and/or presence of defects, which also tends to shift the region of the columnar phase to lower temperature. In addition to these two above-mentioned effects, a competing effect induced by surface ordering can lead to an increase of the transition temperature.[45] The resulting variation of the phase transition temperature with the pore size has been also discussed for calamitic liquid crystals.[44] In more drastic conditions of confinement, the unidirectional field induced by the coupling of the order parameter to the confining media can drive the character of the nematic-to-isotropic transition from first to second order.[35]

The emphasis of the hysteretic behavior and the sharp transition for the Py4CEH in AAO membranes indicate that the Col$_h$−Iso transition retains a first-order character. The width of the hysteresis loop, which is less than 1 K for the bulk, is about 14 and 9 K in AAO50 for SANS and X-ray experiments, respectively. The appearance of a hysteretic behavior has been discussed for the freezing-melting of simple solvents confined in controlled pore glasses with different size.[47] It has been associated to the role of the interfacial liquid−solid energy in the free energy of the confined phase and the existence of different pathways for freezing and melting. This model predicts a ratio between the melting and freezing temperature depression equal to 1/2 for materials confined in a cylindrical geometry. A smaller value of this ratio can be obtained for Py4CEH confined in AAO50 (Table 3).

The larger hysteresis observed for Py4CEH can be attributed to nucleation factors which are not covered by this model. Nucleation factors extend the region of metastability of the isotropic phase on cooling. In the case of crystalline materials, it is commonly stated that the melting point depression can be related to thermodynamic considerations expressed by the Gibbs−Thomson equation or related models.[48] On the contrary, the freezing point can be shifted downward significantly below the thermodynamic prediction.[49] This phenomenon has been expressed by Morishige et al. as genuine supercooling (dynamical supercooling) as opposed to the Gibbs−Thomson effect (thermodynamic supercooling), which defines the lower limit of the hysteresis width.[50] Genuine supercooling has been attributed to the presence of a kinetic barrier to crystallization. Petrov et al.[47] have shown that the melting depression takes an exact and rigorous value, provided that the confined liquid is in equilibrium with a crystalline bulk reservoir. Otherwise, experimental factors affecting the nucleation mechanism (thermal history, thermal rate, absence of a frozen bulk outside the pores) can modify the extent of genuine supercooling. Both phenomena are observed for first-order Col$_h$−Iso transition in AAO-confined DCLC. During the heating scans, Col$_h$−Iso transition temperature takes almost the same value whatever the technique used. On the contrary, genuine supercooling is evidenced during cooling scans leading to a wider dispersion of the depression of the transition temperatures (about 5 K) among the different samples and methods used.

The silanization of the pore surface of AAO50 membranes leads to a more pronounced downward shift of the Col$_h$−Iso transition than for native alumina. The transition is also more abrupt for grafted AAO50 than for native AAO50. In the grafted alumina, the reduction of the pore size induced by the presence of trimethylsilyl groups is too small to account for these observations. Indeed, we infer that this result more probably reflects the importance of the surface interaction in the surface ordering and the thermal stability of the confined Col$_h$ phase.

Unlike Py4CEH-AAO materials, the evolution of the Bragg peak of Py4CEH-pSi sample is not sharp but exhibits a gradual temperature variation during cooling. The Bragg peak sharpens and shifts continuously to lower q values while cooling down (parts b and c of Figure 8). The values reached at the lowest temperature studied (305 K) remain higher than those reached in the $\mathrm{Col_h}$ phase in the case of Py4CEH-AAO samples. The observed gradual growth of short-range correlations over an extended temperature range shares some similarities with the behavior of smectics in porous silicon.[19] Porous silicon materials with pore size as small as 8 nm introduce dominant finite size effects and large surface curvature that inhibit the growth of ordered columnar domains. This tendency is amplified by the roughness of porous silicon walls. In the case of rodlike molecules, it has been shown that the confinement effects of porous silicon on the structure and the phase transition of liquid crystal were markedly different from the one observed for AAO membranes. These features have been related to the quenched disorder effects induced by highly corrugated inner surfaces.[19,20,35,36]

CONCLUSION

The aim of the present work was to investigate the modifications of the structure and the phase transition behavior of a discotic columnar liquid crystal induced by confinement in nanochannels. AAO membranes with three different pore diameters (25, 50, 200 nm), silanized and native, as well as porous silicon (pores of 8 nm) were used in order to disentangle the effects of pore size, surface interaction, and surface roughness. SANS and X-ray diffraction experiments of DCLC embedded in aligned nanopores provide a direct access to the organization and orientation of the columnar phase likewise to the nature of the phase transition behavior, which was investigated by the temperature ramp.

The structure of Py4CEH in AAO membranes is dominated by a homeotropic anchoring. In cylindrical geometry, this surface condition competes with the formation of a hypothetical defect-free single domain that would be possible with a parallel axial arrangement of columns. This phenomenon is amplified for the smallest pores. However an improved texture can be obtained after hydrophobic treatment of the pore surface leading to a preferred orientation of the 6-fold axis with respect to the pore axis.

Results of particular interest concern the phase transition behavior. Confinement in AAO membranes induces a large melting depression of the $\mathrm{Col_h}$−Iso transition and the appearance of a hysteretic character. The smaller the pore size is, the stronger both effects are. While these features are qualitatively similar to what has been commonly reported in terms of cryoporometry for the freezing−melting of simple molecules, the amplitude of this effect is strikingly amplified for DCLC. The obtained results demonstrate the importance of surface anchoring and topological constrains, which can occur in the nucleation process and the relative stability of confined phases in the case of DCLC.

In the case of porous silicon, the gradual increase of short-range columnar correlations in place of the bulk discontinuous $\mathrm{Col_h}$−Iso transition compares well with results obtained for rod-like liquid crystals. This case highlights that the disorder effects induced by the drastic conditions of confinement (<10 nm) and the highly corrugated inner surface of porous silicon, which were initially reported for nematics and smectics, are also critical issues for confined discotics.

It is worth mentioning the recent observation of a glassy dynamics in bulk Py4CEH by dielectric relaxation and specific heat spectroscopy.[52] This interesting result would benefit from a further investigation of the molecular dynamics of this DCLC in the confined state. Besides its fundamental interest, the conclusions drawn by this study may have technological implications. Indeed, it is noteworthy that the planar anchoring of DCLC materials under confinement is the most appropriate for the efficient use of nanowires as semiconducting materials. At variance, our study has demonstrated that in the case of AAO a homeotropic anchoring was favored. The interaction of DCLC with the pore surface is obviously the driving force for the orientation of columnar phase. It underlines that efforts focused on this issue could help making progress in the effective integration of DCLC nanowires in technological devices.

AUTHOR INFORMATION

Corresponding Author

*E-mail: denis.morineau@univ-rennes1.fr.

Notes

The authors declare no competing financial interest.

ACKNOWLEDGMENTS

The authors thank N. Gautier and J. Le Lannic for transmission and scanning electron micrographs, respectively, and J. Kelber and Dr H. Bock for providing us with sample materials. The authors acknowledge financial support by the joint ANR DFG program "TEMPLDISCO" Grant No. ANR-09-BLAN-0419.

REFERENCES

(1) Shirota, Y. *J. Mater. Chem.* **2000**, *10* (1), 1−25.

(2) Sergeyev, S.; Pisula, W.; Geerts, Y. H. *Chem. Soc. Rev.* **2007**, *36* (12), 1902−1929.

(3) Feng, X. L.; Marcon, V.; Pisula, W.; Hansen, M. R.; Kirkpatrick, J.; Grozema, F.; Andrienko, D.; Kremer, K.; Mullen, K. *Nat. Mater.* **2009**, *8* (5), 421−426.

(4) Laschat, S.; Baro, A.; Steinke, N.; Giesselmann, F.; Haegele, C.; Scalia, G.; Judele, R.; Kapatsina, E.; Sauer, S.; Schreivogel, A.; Tosoni, M. *Angew. Chem., Int. Ed.* **2007**, *46* (26), 4832−4887.

(5) Schmidt-Mende, L.; Fechtenkotter, A.; Mullen, K.; Moons, E.; Friend, R. H.; MacKenzie, J. D. *Science* **2001**, *293* (5532), 1119−1122.

(6) Karthaus, O.; Ringsdorf, H.; Tsukruk, V. V.; Wendorff, J. H. *Langmuir* **1992**, *8* (9), 2279−2283.

(7) De Cupere, V.; Tant, J.; Viville, P.; Lazzaroni, R.; Osikowicz, W.; Salaneck, W. R.; Geerts, Y. H. *Langmuir* **2006**, *22* (18), 7798−7806.

(8) Grelet, E.; Bock, H. *Europhys. Lett.* **2006**, *73* (5), 712−718.

(9) Hatsusaka, K.; Ohta, K.; Yamamoto, I.; Shirai, H. *J. Mater. Chem.* **2001**, *11* (2), 423−433.

(10) Pisula, W.; Tomovic, Z.; El Hamaoui, B.; Watson, M. D.; Pakula, T.; Mullen, K. *Adv. Funct. Mater.* **2005**, *15* (6), 893−904.

(11) Thiebaut, O.; Bock, H.; Grelet, E. *J. Am. Chem. Soc.* **2010**, *132* (20), 6886−6887.

(12) Grelet, E.; Dardel, S.; Bock, H.; Goldmann, M.; Lacaze, E.; Nallet, F. *Eur. Phys. J. E* **2010**, *31* (4), 343−349.

(13) Schweicher, G.; Gbabode, G.; Quist, F.; Debever, O.; Dumont, N.; Sergeyev, S.; Geerts, Y. H. *Chem. Mater.* **2009**, *21* (24), 5867−5874.

(14) Pouzet, E.; De Cupere, V.; Heintz, C.; Andreasen, J. W.; Breiby, D. W.; Nielsen, M. M.; Viville, P.; Lazzaroni, R.; Gbabode, G.; Geerts, Y. H. *J. Phys. Chem. C* **2009**, *113* (32), 14398−14406.

(15) Brunet, T.; Thiebaut, O.; Charlet, E.; Bock, H.; Kelber, J.; Grelet, E. *EPL* **2011**, *93* (1), 16004.

(16) Steinhart, M.; Zimmermann, S.; Goring, P.; Schaper, A. K.; Gosele, U.; Weder, C.; Wendorff, J. H. *Nano Lett.* **2005**, *5* (3), 429−434.

(17) Alba-Simionesco, C.; Coasne, B.; Dosseh, G.; Dudziak, G.; Gubbins, K. E.; Radhakrishnan, R.; Sliwinska-Bartkowiak, M. *J. Phys.: Condens. Matter* **2006**, *18* (6), R15−R68.

(18) Richert, R. *Annu. Rev. Phys. Chem.* **2011**, *62*, 65−84.

(19) Guegan, R.; Morineau, D.; Lefort, R.; Beziel, W.; Guendouz, M.; Noirez, L.; Henschel, A.; Huber, P. *Eur. Phys. J. E* **2008**, *26* (3), 261−273.
(20) Guegan, R.; Morineau, D.; Loverdo, C.; Beziel, W.; Guendouz, M. *Phys. Rev. E* **2006**, *73* (1), 011707.
(21) Chahine, G.; Kityk, A. V.; Demarest, N.; Jean, F.; Knorr, K.; Huber, P.; Lefort, R.; Zanotti, J. M.; Morineau, D. *Phys. Rev. E* **2010**, *82* (1), 011706.
(22) Prasad, S. K.; Sridevi, S.; Rao, D. S. S. *J. Phys. Chem. B* **2010**, *114* (22), 7474−7481.
(23) Werner, J.; Otto, K.; Enke, D.; Pelzl, G.; Janowski, F.; Kresse, H. *Liq. Cryst.* **2000**, *27* (10), 1295−1300.
(24) Stillings, C.; Martin, E.; Steinhart, M.; Pettau, R.; Paraknowitsch, J.; Geuss, M.; Schmidt, J.; Germano, G.; Schmidt, H. W.; Gosele, U.; Wendorff, J. H. *Mol. Cryst. Liq. Cryst.* **2008**, *495*, 637−645.
(25) Stillings, C.; Pettau, R.; Wendorff, J. H.; Schmidt, H. W.; Kreger, K. *Macromol. Chem. Phys.* **2010**, *211* (2), 250−258.
(26) Kopitzke, J.; Wendorff, J. H.; Glusen, B. *Liq. Cryst.* **2000**, *27* (5), 643−648.
(27) Hassheider, T.; Benning, S. A.; Kitzerow, H. S.; Achard, M. F.; Bock, H. *Angew. Chem., Int. Ed.* **2001**, *40* (11), 2060−2063.
(28) Ba, L.; Li, W. S. *J. Phys. D: Appl. Phys.* **2000**, *33* (20), 2527−2531.
(29) Jessensky, O.; Muller, F.; Gosele, U. *Appl. Phys. Lett.* **1998**, *72* (10), 1173−1175.
(30) Li, A. P.; Muller, F.; Birner, A.; Nielsch, K.; Gosele, U. *J. Appl. Phys.* **1998**, *84* (11), 6023−6026.
(31) Li, A. P.; Muller, F.; Birner, A.; Nielsch, K.; Gosele, U. *Adv. Mater.* **1999**, *11* (6), 483−487.
(32) Dantras, E.; Dandurand, J.; Lacabanne, C.; Laffont, L.; Tarascon, J. M.; Archambeau, S.; Seguy, I.; Destruel, P.; Bock, H.; Fouet, S. *Phys. Chem. Chem. Phys.* **2004**, *6* (16), 4167−4173.
(33) Masuda, H.; Fukuda, K. *Science* **1995**, *268* (5216), 1466−1468.
(34) Smith, R. L.; Collins, S. D. *J. Appl. Phys.* **1992**, *71* (8), R1−R22.
(35) Kityk, A. V.; Wolff, M.; Knorr, K.; Morineau, D.; Lefort, R.; Huber, P. *Phys. Rev. Lett.* **2008**, *101* (18), 187801.
(36) Chahine, G.; Kityk, A. V.; Knorr, K.; Lefort, R.; Guendouz, M.; Morineau, D.; Huber, P. *Phys. Rev. E* **2010**, *81* (3), 031703.
(37) Ji, Q.; Lefort, R.; Morineau, D. *Chem. Phys. Lett.* **2009**, *478* (4−6), 161−165.
(38) Henschel, A.; Kumar, P.; Hofmann, T.; Knorr, K.; Huber, P. *Phys. Rev. E* **2009**, *79* (3), 032601.
(39) Henschel, A.; Hofmann, T.; Huber, P.; Knorr, K. *Phys. Rev. E* **2007**, *75* (2), 021607.
(40) Henschel, A.; Huber, P.; Knorr, K. *Phys. Rev. E* **2008**, *77* (4), 042602.
(41) Jackson, C. L.; McKenna, G. B. *J. Chem. Phys.* **1990**, *93* (12), 9002−9011.
(42) Zheng, W.; Simon, S. L. *J. Chem. Phys.* **2007**, *127* (19), 194501-1−194501-11.
(43) Cramer, C.; Cramer, T.; Kremer, F.; Stannarius, R. *J. Chem. Phys.* **1997**, *106* (9), 3730−3742.
(44) Iannacchione, G. S.; Finotello, D. *Phys. Rev. E* **1994**, *50* (6), 4780−4795.
(45) Grigoriadis, C.; Duran, H.; Steinhart, M.; Kappl, M.; Butt, H. J.; Floudas, G. *ACS Nano* **2011**, *5* (11), 9208−9215.
(46) Alcoutlabi, M.; McKenna, G. B. *J. Phys.: Condens. Matter* **2005**, *17* (15), R461−R524.
(47) Petrov, O. V.; Furo, I. *Microporous Mesoporous Mater.* **2010**, *136* (1−3), 83−91.
(48) Christenson, H. K. *J. Phys.: Condens. Matter* **2001**, *13* (11), R95−R133.
(49) Xia, Y. D.; Dosseh, G.; Morineau, D.; Alba-Simionesco, C. *J. Phys. Chem. B* **2006**, *110* (39), 19735−19744.
(50) Morishige, K.; Kawano, K. *J. Chem. Phys.* **2000**, *112* (24), 11023−11029.
(51) Crawford, G. P.; Steele, L. M.; Ondriscrawford, R.; Iannacchione, G. S.; Yeager, C. J.; Doane, J. W.; Finotello, D. *J. Chem. Phys.* **1992**, *96* (10), 7788−7796.
(52) Krause, C.; Yin, H.; Cerclier, C.; Morineau, D.; Wurm, A.; Schick, C.; Emmerling, F.; Schönhals, A. *Soft Matter* **2012**, DOI: 10.1039/C2SM25610J.